Personalized Keystroke Dynamics for Self-Powered Human–Machine Interfacing

Jun Chen,[†,⊥] Guang Zhu,[†,§,⊥] Jin Yang,[†,‡,⊥] Qingshen Jing,[†] Peng Bai,[†] Weiqing Yang,[†] Xuewei Qi,[#] Yuanjie Su,[†] and Zhong Lin Wang[*,†,§]

[†]School of Materials Science and Engineering, Georgia Institute of Technology, Atlanta, Georgia 30332-0245, United States, [§]Beijing Institute of Nanoenergy and Nanosystems, Chinese Academy of Sciences, Beijing 100083, China, [‡]Department of Optoelectronic Engineering, Chongqing University, Chongqing 400044, China, and [#]Department of Electrical Engineering, University of California, Riverside, California 92521, United States. [⊥]J.C., G.Z., and J.Y. contributed equally.

ABSTRACT The computer keyboard is one of the most common, reliable, accessible, and effective tools used for human–machine interfacing and information exchange. Although keyboards have been used for hundreds of years for advancing human civilization, studying human behavior by keystroke dynamics using smart keyboards remains a great challenge. Here we report a self-powered, non-mechanical-punching keyboard enabled by contact electrification between human fingers and keys, which converts mechanical stimuli applied to the keyboard into local electronic signals without applying an external power. The intelligent keyboard (IKB) can not only sensitively trigger a wireless alarm system once gentle finger tapping occurs but also trace and record typed content by detecting both the dynamic time intervals between and during the inputting of letters and the force used for each typing action. Such features hold promise for its use as a smart security system that can realize detection, alert, recording, and identification. Moreover, the IKB is able to identify personal characteristics from different individuals, assisted by the behavioral biometric of keystroke dynamics. Furthermore, the IKB can effectively harness typing motions for electricity to charge commercial electronics at arbitrary typing speeds greater than 100 characters per min. Given the above features, the IKB can be potentially applied not only to self-powered electronics but also to artificial intelligence, cyber security, and computer or network access control.

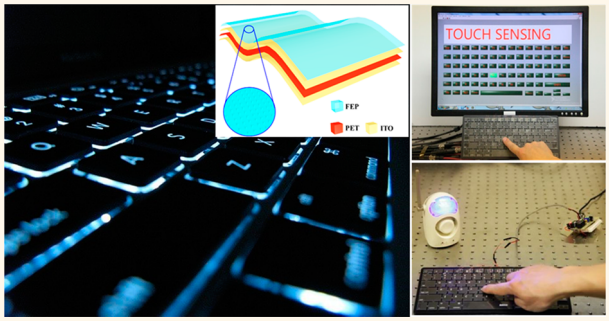

KEYWORDS: triboelectrification · IKB · self-powering · human–machine interfacing · keystroke dynamics · biometrics

Computers are practically indispensable pieces of equipment that many of us rely on each day. Accessing the information provided by computers from the Internet dictates the quality, efficiency, and happiness of our work and life. A keyboard, an indispensable component of the system, is the only means for information input and control for many purposes, such as information recording/outputting, financial management, bill payment, personal communications, and many more. In this regard, our heavy reliance on computers incurs a major concern for security issues. A breach of information security due to unauthorized access to computers will widely jeopardize people's normal lives, business development, company operation, and even national security.[1−3] Conventional security measures such as personal identification numbers, tokens, or passwords can provide only limited protection, since they themselves are subject to illegitimate activities. Therefore, as we are moving into paperless work, an advanced and general approach that can provide multi-fold protection to computer systems is highly desired.

Here we develop an intelligent, self-powered keyboard as an advanced safeguard against unauthorized access to computers. Based on contact electrification, which is ubiquitous but underexplored,[4−10] between human fingers and keys, the intelligent keyboard (IKB) converts typing motions on the keyboard into locally electric signals that can be harnessed for either touch-sensing or energy-harvesting purposes. Most significantly, the IKB allows a direct identification of personality in data input using the dynamic electronic signals generated when striking keys.

First, through integration of the IKB with a signal-processing circuit, a complete

* Address correspondence to zhong.wang@mse.gatech.edu.

Received for review December 1, 2014 and accepted December 30, 2014.

Published online December 30, 2014
10.1021/nn506832w

touch-sensing system was built up. A wireless alarm is triggered once a finger gently taps on a key. Furthermore, each key is individually addressable, which enables tracing and recording the typing content in real time. This capability will provide administrators with great convenience for identifying impostors or intruders, and it will have extensive applications in keyboard-based information security.

More importantly, a fatal weakness of the current authentication systems is that an identity thief can easily pass as the genuine owner with stolen personal identification information (*e.g.*, passwords).[1−3,11] Improvements regarding this issue can hardly be accomplished without having better identifiers that preferably cannot be easily separated from the owner of the computer. Thus, the behavioral biometric of keystroke dynamics, which was first considered as a means of distinguishing typists in the mid-1970s, can be harnessed to place an additional layer of security on existing systems, since biometric identifiers are intrinsic and harder to separate or mimic from the genuine owner. Immediately after Gaines *et al.* presented a preliminary study on keystroke dynamic-based authentication using the T-test on digraph features,[12] the use of keystroke dynamics for verification and identification purposes was extensively investigated, since they are inexpensive and less intrusive and can be implemented easily on top of the current authentication systems without major modification.[13,14] However, keystroke dynamics has developed rather slowly and is still at its very early stage, partially because almost all of the proposed studies rely on dimensional keystroke timing vectors as typing patterns, which can only communicate the keystroke timing characteristics, thus rendering this biometric measure lacking in universality, uniqueness, permanence, accuracy, and acceptability.[15−18] A breakthrough is desperately needed to obtain a unique and permanent typing pattern that can be used as an effective identifier/calibration for practical applications. In this work, the typing-induced electric signals can not only differentiate keystroke timing but also quantitatively record concrete dynamic changes in the course of typing using the self-generated electric current and voltage signals. It offers an unprecedentedly accurate, unique, and permanent typing pattern for further verification and recognition purposes. Meanwhile, Daubechies Wavelet of order 4 (DB4) was employed to successfully classify and identify the typing patterns. More importantly, with reliance on the obtained typing patterns, a biometric authentication system was established. Compared with the state-of-the-art biometric techniques,[19,20] a remarkably lower Equal Error Rate (EER) value of 1.34% was achieved at the threshold of 0.37.

Furthermore, the proposed keyboard can also convert mechanical energy from human typing into electricity. With an area power density of 69.6 μW cm^{-2}, the keyboard can effectively harness the typing motions to generate electricity and to charge small electronics at arbitrary typing speed greater than 100 characters per min (CPM), a giant leap compared to previous reports.[21] Last but not least, holding a surface contact angle of 160° and a sliding angle of 7.2° ± 0.5°due to surface nanostructure modification, the IKB is also an effective self-cleaner, which keeps itself free of dirt and grime.[22−24] Even a sweaty hand can barely degrade the output performance, and the IKB is also easily cleaned up if contamination occurs.

Given such features as self-securing, self-powering, and self-cleaning, as well as unique applicability resulting from distinctive mechanism and one-piece non-mechanical-punching structure, the IKB presented in this work is a practical approach in converting typing motions for self-powered electronics as well as a milestone in the development toward a highly secure behavioral biometrics-based authentication system, which will have extensive applications in the fields of artificial intelligence, cyber security, and computer or network access control.

RESULTS AND DISCUSSION

Device Structure. The key functional element (KFE) of the IKB is composed of vertically stacked transparent thin film materials. A layer of polyethylene terephthalate (PET) sits between two layers of ITO that are the bottom and the top electrodes. Then, a layer of fluorinated ethylene propylene (FEP) is applied onto the ITO surface as an electrification layer that generates triboelectric charges upon contact with human fingers, as schematically shown in Figure 1a. FEP nanowires arrays were created on the exposed FEP surface by a top-down method through reactive ion etching.[25] A scanning electron microscopy (SEM) image of vertically aligned FEP nanowires is displayed in Figure 1b, which indicates that the average clustering diameter of FEP nanowires is 104 ± 21 nm with an average length of 0.8 ± 0.2 μm. The static contact angle of the FEP surface was measured by a sessile droplet method with a 2 μL water droplet. The inset of Figure 1b shows the contour of the resting droplet, which indicates a contact angle of 160° by Young−Laplace fitting. Meanwhile, a tilting base method was employed to investigate the surface sliding angle of the IKB. A schematic illustration of the setup for sliding angle measurement is demonstrated in Supporting Figure S1. A sliding angle of 7.2° ± 0.5° was experimentally observed. The superhydrophobicity of the IKB surface assures its self-cleaning property, which can effectively keep the keyboard free of dirt and grime. A photograph of an as-fabricated KFE is shown in Figure 1c,d, plainly demonstrating its flexibility, transparency, and one-piece structure without mechanical punching. Figure 1e is a photograph of an IKB after assembling the KFE with a commercial keyboard. As discussed in Methods, the fabrication

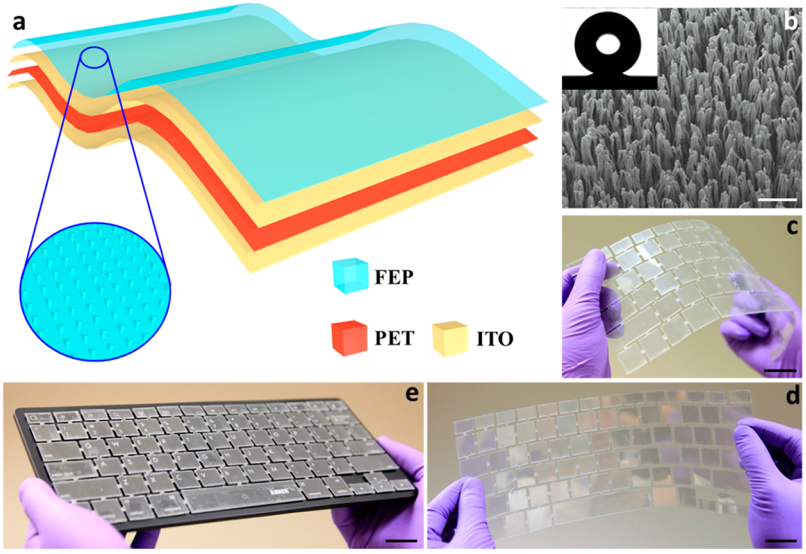

Figure 1. Structural design of the KFE of the intelligent keyboard. (a) Schematic illustrations of the KFE. Inset: Enlarged schematic of FEP nanowires on the top surface. It is noted that these drawings do not scale. (b) SEM image of FEP nanowires. Inset: Contour of resting droplet for surface static contact angle measurement. The scale bar is 500 nm. (c,d) Photograph of a flexible and transparent KFE. The scale bars are 3 cm. (e) Photograph of an as-fabricated IKB, which is a system integration of KFE and a commercial keyboard. The scale bars are 3 cm.

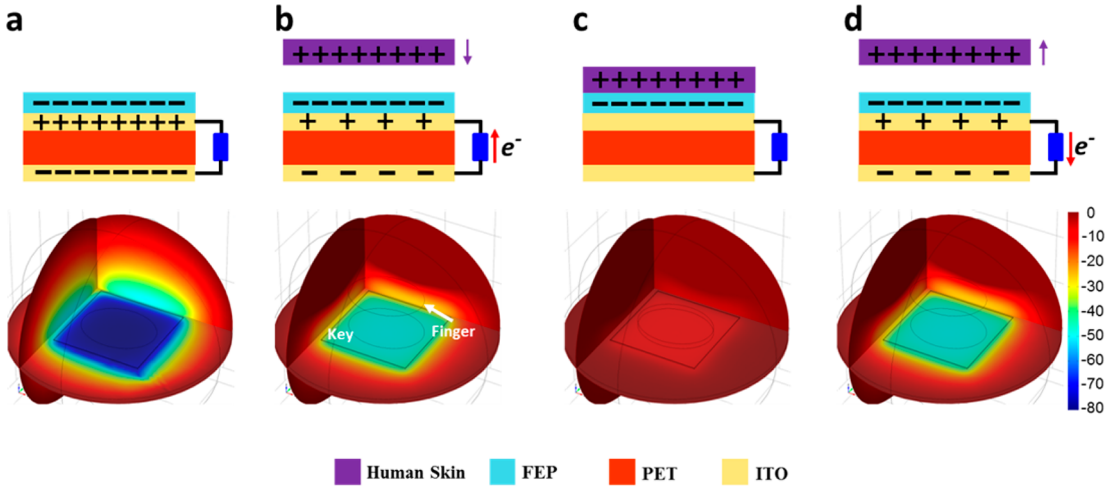

Figure 2. Schematics of operating principle of the intelligent keyboard. Both two-dimensional schematic illustrations of charge distribution (up) and three-dimensional potential distribution by COMSOL (down) were employed to elucidate the working principle of IKB. (a) Initial state in which the FEP is negatively charged after contact with human finger. (b) When a keystroke is initiated, the approach of positively charged human finger results in free electrons flowing from bottom ITO electron to top electrode. (c) The current in the external circuit lasts until the human finger fully contacts with FEP. (d) When the finger is up and a separation occurs, it produces another current in the external circuit flowing from the bottom electrode to top electrode.

process of the KFE is straightforward and compatible with possible large-scale manufacturing.

Electrical Signals Generation Process. The basic working principle of the IKB is based on the coupling between contact electrification and electrostatic induction rather than the traditional mechanical switching. An electricity generation process from a key unit is depicted in Figure 2. Here, both two-dimensional schematic illustrations of charge distribution (up) and three-dimensional potential distribution by COMSOL (down) were used for illustration. When a human finger is brought into contact with FEP, charge transfer at the contact interface occurs. According to the triboelectric series,[26] electrons are injected from human skin into FEP, since FEP is much more triboelectrically negative than human skin, generating positive triboelectric charges on the human skin and negative ones on the FEP.[27−35] Subsequently, if the human finger moves away, the negative charges on the FEP side will induce positive charges on the top ITO electrode and thus equal amount of negative charges on the bottom electrode (Figure 2a). Once a keystroke is initiated, the positively charged human finger approaches the keyboard, the induced positive charges on the top

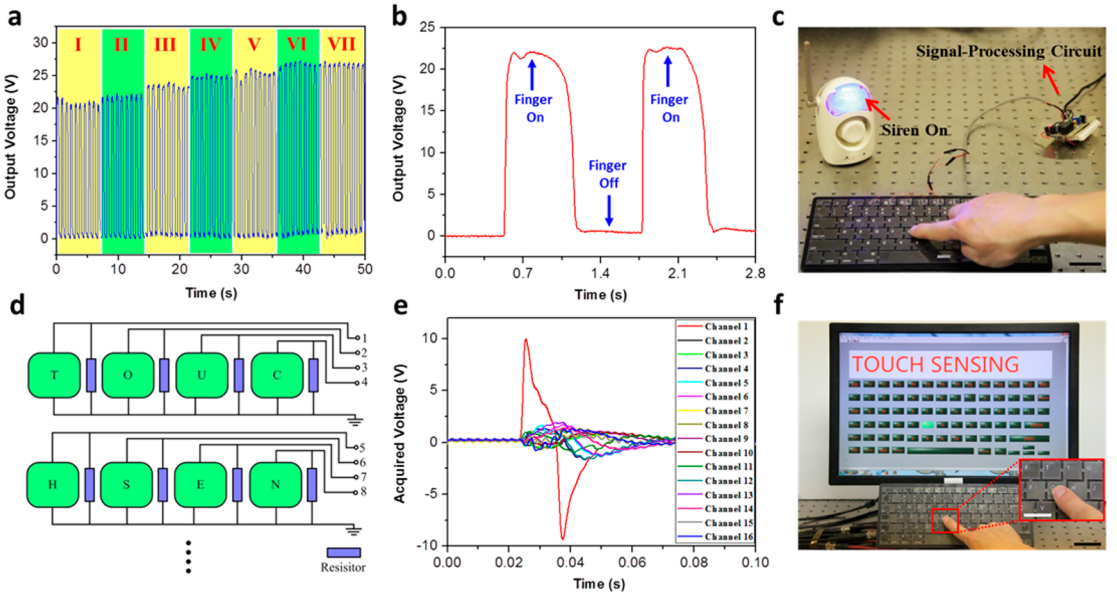

Figure 3. Intelligent keyboard as a self-securing system. (a) Measured output voltage is an increasing function of the key dimensions when a gentle keystroke was applied. (b) An enlarged view of obtained output voltage when the smallest key is gently touched. (c) Triggering a wireless alarm system by gentle finger tapping on the IKB. The scale bar is 5 cm. (d) Schematic diagram of keyboard-based multi-channel data acquisition system for keystroke tracing and real-time recording. (e) The system acquired output voltage signals when the key "T" was stroked. (f) An photograph demonstrated the IKB for the real-time keystroke tracing and recording. A continuously typing string "TOUCH SENSING" was recorded in real time without uncomfortable delay. The scale bar is 5 cm. Inset: Enlarged view of the key "G" being stroked. The scale bar is 2 cm.

electrode are expelled, resulting in a flow of free electrons from the bottom electrode to top electrode (Figure 2b) until the finger and the key are in contact (Figure 2c). When the finger separates, free electrons flow backward from the top electrode to the bottom electrode (Figure 2d). This is a full cycle of the electricity-generating process. It is worth noting that the triboelectric charges do not dissipate but remain on the FEP surface for an extended period of time.[36−44] Consequently, consecutive keystrokes result in a periodical-changing electric field that drives reciprocating flows of electrons between electrodes. The variation of electric potential is visualized *via* COMSOL in Supporting Movie 1.

Intelligent Keyboard as a Self-Securing System. The keyboard was integrated with a signal-processing circuit to develop a complete wireless warning system. The circuit diagram of the complete IKB-based self-securing system is shown in Supporting Figure S2. This customized circuit for the IKB holds two unique advantages. First, a designed trigger voltage threshold of 5 V enables the IKB to work stably even in a high electrical noise environment. Second, the alarm time is controllable and tunable by the signal-processing circuit. Once a finger gently strokes a key, the generated voltage signal triggers an IC timer that controls a wireless transmitter and remotely switches a siren between a panic state and a silence state. The keys in the keyboards are categorized into seven regions (Supporting Figure S3) according to their dimensions to compare their output voltage. The obtained results are shown in Figure 3a. An increasing function between key dimensions and the output voltage is observed. The reason is that contact electrification is a surface charging effect, a larger amount of triboelectric charges will contribute to a higher voltage output.[45] Figure 3b is an enlarged view of the output voltage when the smallest key is gently touched. Even this lowest voltage was capable of triggering the siren that produced a sharp alarm with flashing light (Figure 3c, Supporting Movie 2).

Furthermore, a customized multi-channel data acquisition system was designed for the IKB to individually address the electric signal from each key (Figure 3d). Consequently, the real-time tracing and recording during typing can be realized. Every channel was electrically but independently connected to a key in the keyboard as a functional unit, and each unit was connected to the ground through a 1 MΩ resistor. When a keystroke was initiated on a particular key, "T" for example, a peak output voltage up to 10 V was acquired from the corresponding channel, while signals from other keys were less than 2.5 V (Figure 3e). Theoretically, the signals from untouched keys should be 0. However, a certain voltage signals were observed experimentally, which is mainly due to the coupling among all of the channels in the data acquisition system.[46,47]

For recognition purpose, the maximum peak value of the output voltage from channel i, V_{pi}, was extracted. Then the threshold voltage V_{th} can be analytically expressed by the following equation using Pauta

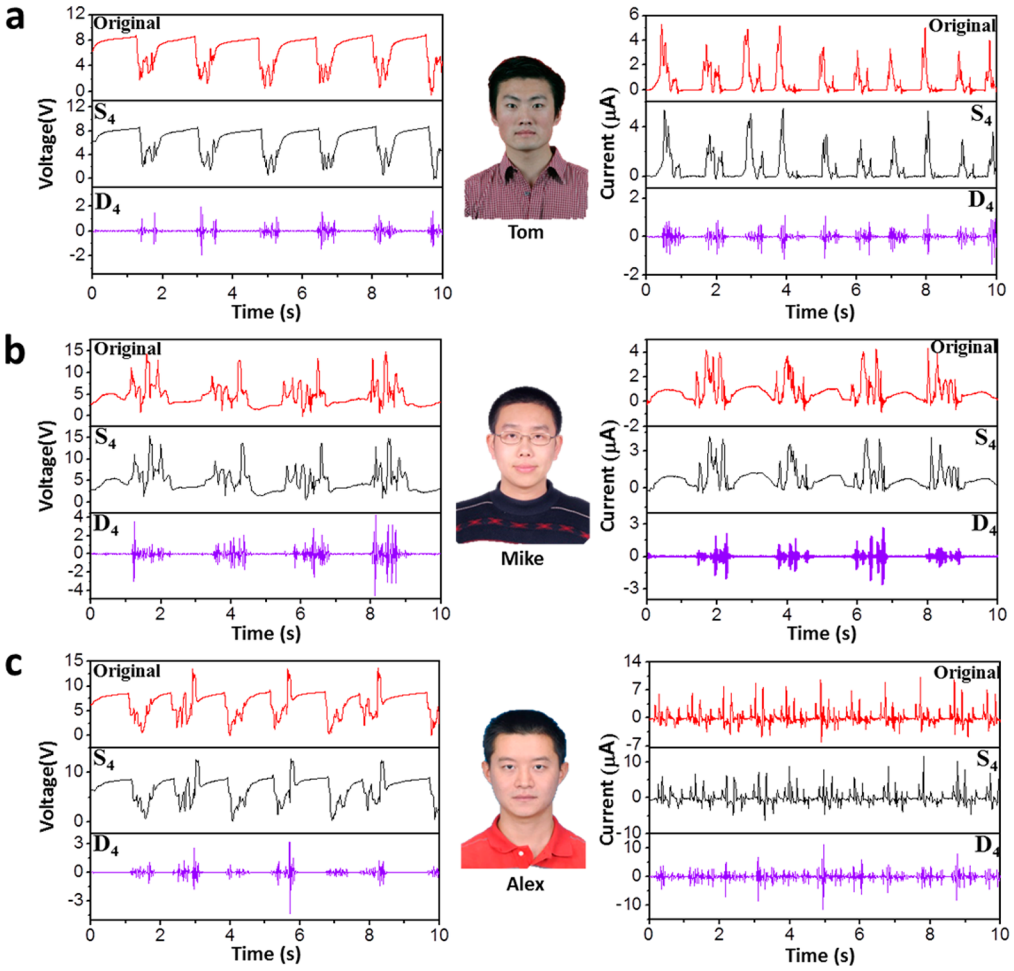

Figure 4. Personality identified keystroke dynamics using intelligent keyboard. Typing patterns obtained when (a) Tom, (b) Mike, and (c) Alex were repeatedly typing the word "touch" more than four times into the computer *via* the IKB. S4 and D4 are the corresponding wavelet components after DB4 transformation.

Criterion Method (the detailed modeling is presented in Supporting Note S1):

$$V_{th} = \frac{1}{n}\sum_{i=1}^{n} V_{pi} + \frac{3}{\sqrt{n}}\sqrt{\sum_{i=1}^{n} V_{pi}(V_{pi} - 1)} \qquad (1)$$

where n is the total number of channels, and i is integrated from 1 to n. Once the extracted V_{pi} is higher than V_{th}, the key corresponding to this particular channel is considered to be stroked. Figure 3f demonstrates the real-time keystroke tracing and recording. When a phrase "TOUCH SENSING" was continuously typed, it was simultaneously recorded and displayed without noticeable delay (Supporting Movie 3). As shown in Supporting Figure S4 and Supporting Movie 4, any typing content applies.

Intelligent Keyboard for Keystroke Dynamics. Typing patterns based on dimensional keystroke timing vector, lacking uniqueness and permanence, largely hinder the practicality and acceptability of the behavioral biometric of keystroke dynamics as an effective identifier for current authentication systems. The IKB in this work provides a superior route in creating accurate, unique, and permanent typing patterns for verification and identification purposes. As demonstrated in Figure 4a–c, three sets of original typing patterns (in red curves) were respectively obtained for three typists, Tom, Mike, and Alex, who independently typed the word "touch" for more than four times on the IKB in each accustomed manner. Each set of typing pattern corresponds to two subsets of characteristic signals (voltage and current), which are time-series data. These electric signals correlate to a variety of information, including the manner and rhythm of the keystroke, typing habit, finger size, individual bioelectricity, and applied typing force. Thus, they can not only characterize the keystroke timing, but also quantitatively record the concrete dynamic changes in the course of typing.

The as-collected electric signals look apparently different from each other. For quantitative differentiation, Discrete Fourier Transformation (DFT) was performed to obtain frequency features of the electric signals. As shown in Supporting Figure S5, the frequency spectra of the voltage and the current from different individuals are distinct in term of the position

TABLE 1. Pearson Correlation Coefficients between the Wavelet Components of the Typing Patterns

	Tom		Mike		Alex			Tom		Mike		Alex	
Voltage	S_4	D_4	S_4	D_4	S_4	D_4	current	S_4	D_4	S_4	D_4	S_4	D_4
Tom	0.91	0.92	0.43	0.45	0.45	0.43	Tom	0.92	0.89	0.44	0.41	0.42	0.39
Mike	0.43	0.45	0.86	0.87	0.42	0.34	Mike	0.42	0.41	0.85	0.85	0.36	0.35
Alex	0.45	0.43	0.42	0.34	0.88	0.89	Alex	0.42	0.39	0.36	0.35	0.88	0.89

and amplitude of the major signal components (Supporting Table S1). Furthermore, Wavelet transformation was further carried out to simultaneously obtain both time domain and frequency domain features of the typing patterns. Based on DB4,[48] the typing patterns in the form of electric signals can be expressed by the following formula *via* multi-resolution analysis:

$$f(t) = S_4(t) + D_4(t) + D_3(t) + D_2(t) + D_1(t) \quad (2)$$

and

$$S_4 = \sum_k s_{4,k}\varphi_{4,k}(t) \quad (3)$$

$$D_j = \sum_k d_{j,k}\psi_{j,k}(t) \quad (4)$$

where $s_{4,k}$ and $d_{j,k}$ are the wavelet coefficients, j =1, 2, 3, 4. k is the number of translations of the wavelet for any given scale. $\varphi_{4,k}(t)$ and $\psi_{j,k}(t)$ are respectively the father and mother wavelets. $f(t)$ is either voltage or current signal of the typing patterns. S_4 is smooth. Wavelet details D_4, D_3, D_2, and D_1 represent a set of voltage or current components that provide representations of the original signals at different resolution levels.

The S_4 and D_4 of the original typing patterns after DB4 are presented in Figure 4a−c, for different individuals. Their higher resolution terms,D_3, D_2, and D_1, are presented in Supporting Figure S6. On the basis of DB4 results, the corresponding higher resolution wavelet components of three individuals are significantly different from each other. Still, Pearson correlation coefficient was utilized to quantitatively measure the correlation between the wavelet components by the following equation:[49]

$$\gamma = \frac{\sum_{i=1}^{n}(t_i - \bar{t})(x_i - \bar{x})}{\sqrt{\sum_{i=1}^{n}(t_i - \bar{t})^2}\sqrt{\sum_{i=1}^{n}(x_i - \bar{x})^2}} \quad (5)$$

where n is the length of compared date sequence, and x is either the voltage or the current sequences after DB4. The obtained Pearson correlation coefficient of D_4 and S_4 components are respectively tabulated in Table 1. All of the Pearson correlation coefficients of the voltage or current components from each individual are larger than 0.85, suggesting superior permanence of the typing patterns, while other Pearson correlation coefficients are less than 0.45 that is indicative of excellent uniqueness among individuals. Therefore, the Pearson correlation coefficient can be harnessed to express the uniqueness and permanence among individual typing patterns. In the meanwhile, the correlation coefficient can also act as a threshold to separate the genuine typing patterns from the impostor typing patterns, if a verification system is established using behavioral biometric of keystroke dynamics.

Intelligent Keyboard for Biometric Authentication. To evaluate the performance of the triboelectrification enabled behavioral biometric of keystroke dynamics as an effective identifier, 104 participants were invited to independently type the word "touch" for more than four times on the IKB in each accustomed manner. All the participants are the randomly and diversely selected with an age span from 14 to 69 years old, male and female people from different countries. All the typing patterns and their corresponding D_4 and S_4 components are demonstrated in the Supporting Figures S7−S32.

Subsequently, a collection of 104 individual typing patterns were divided into 52 client patterns and 52 impostor patterns. In the whole testing set of 104 typing patterns, the user template is composed of the 52 client patterns, and the performance of the authentication biometrics is characterized through two error rates: False Rejection Rate (FRR) and False Acceptance Rate (FAR).

The FRR and FAR are variables depending on the classification threshold. By tuning the threshold, the FRR and FAR can typically be traded off against each other to achieve the preferable classification result. In this regard, the Pearson correlation coefficient was selected as the classification threshold to evaluate the behavioral biometric authentication system using triboelectrification enabled keystroke dynamics. The variation of FAR and FRR in relation to the threshold is shown in Figure 5a. The FRR is increasing with the elevated threshold, while FAR follows a reverse trend. However, the FRR and FAR intersect at a certain threshold value, which indicates the EER point. The inset of Figure 5 is an enlarged view of the EER point of the presented behavioral biometric authentication system. Compared with the state of the art biometric

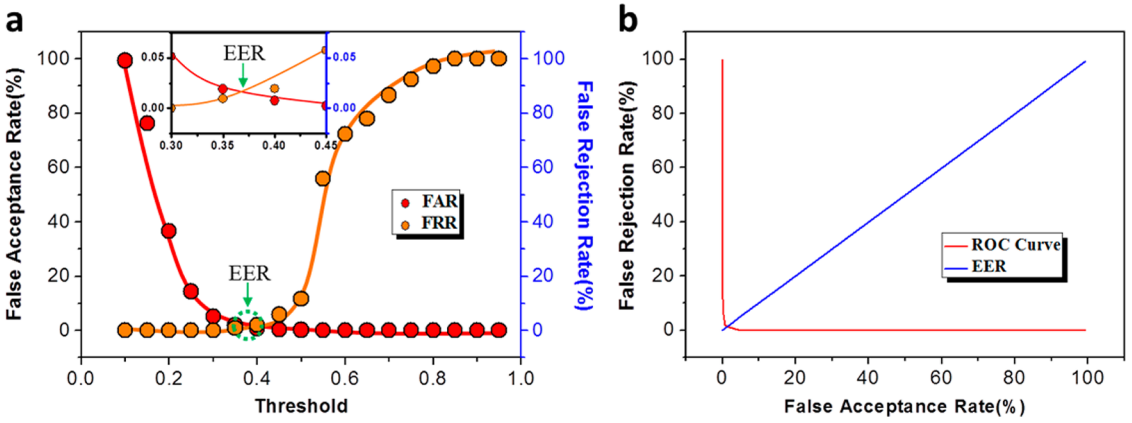

Figure 5. Evaluation of the performance of the biometric authentication system using triboelectrification enabled keystroke dynamics. The variation of FAR and FRR is in relation to the threshold. Inset: Enlarged view of the EER point, which indicates a remarkably low EER value of 1.34% at the threshold of 0.37. (b) Receiver operating characteristic (ROC) curve of the biometric authentication system using triboelectrification enabled keystroke dynamics. The false rejection curve is plotted as a function of the false acceptance curve.

techniques,[19,20] the presented biometric authentication system achieves a remarkably lower EER value of 1.34% at the threshold of 0.37. In the meanwhile, the Receiver Operating Characteristic (ROC) curve is demonstrated in the Figure 5b. In addition, to prove the capability of the IKB as an additional layer of stronger security to current authentication systems, a practical application was demonstrated (Supporting Movie 5). When four different individuals typing the password "touch" into the computer through IKB, only the genuine owner with matched typing pattern can access into the computer. Given its exceptional authentication ability, the IKB is able to identify the personal character of typing individuals, making it practical for developing a highly secured authentication system based on behavioral biometrics.

Intelligent Keyboard for Capturing Wasted Energy. To systematically investigate the performance of the IKB in harvesting typing energy, two typing modes, intermittent and continuous typing, were both evaluated. For the intermittent model, a key in zone II was repeatedly tested because keys in this zone are the mostly used (see Supporting Figure S3 for key classification). The open-circuit voltage and the short-circuit current are exhibited in Figure 6a,b, with peak values of 26.8 V and 23.5 μA. As shown in Figure 6b, the output current is asymmetric. It was found that the larger positive peaks correspond to the process when the key was being pressed, while the smaller ones are produced when the key was being released. Given the same amount of total transported charges, the faster pressing process is expected to generate larger current peaks than the slower releasing process. Resistors were utilized as external loads to further investigate the output power of the IKB. As displayed in Figure 6c, the current amplitude drops with increasing load resistance, while the voltage follows a reverse trend. As a result, as demonstrated in Figure 6d, the instantaneous peak power is maximized at a load resistance of 9 MΩ, which corresponds to a peak power density of 69.6 μW cm^{-2} and a peak specific power of 2.05 mW g^{-1}. This output performance leads previous reports by at least 141 times enhancement.[21] With a diode bridge, the total accumulative induced charges can also be measured, as show in Figure 6e. Each step represents an output current resulting from a keystroke, producing 37 nC of induced charges on average. Correspondingly, the area density of triboelectric charges is calculated to be 134 μC m^{-2}. Such solid achievements are mainly attributed to the following two reasons. First, human skin and FEP have a large difference in triboelectric polarity (Supporting Table S2), which assures large amount of triboelectric charges generated in keystroke. Second, the vertically standing FEP nanowires enables tremendous enhancement of effective contact area as well as triboelectric charges, and thus superior output performance. A detailed interpretation and description of the mechanism behind the nanowires' improved contact area is given in the Contact Area Improvement section.

Meanwhile, the energy harvesting capability of IKB was also evaluated under the continuously typing working mode, which is the mostly used mode for computer users. As demonstrated in Figure 6f, the IKB can effectively capture the wasted typing energy for charging portable electronics in a wide range of typing speeds, which almost covers all kinds of users in daily life. A directly proportional relationship was found between the typing speed and the charging rate. This is because a faster typing means more keystrokes are launched in a unit period of time, thus faster of triboelectric charges generation (Supporting Figure S33), and higher charging rate is expected. Under a moderate typing speed of 350 CPM, a charging rate of 0.019 V s^{-1} was achieved for a commercial capacitor (Supporting Movie 6).

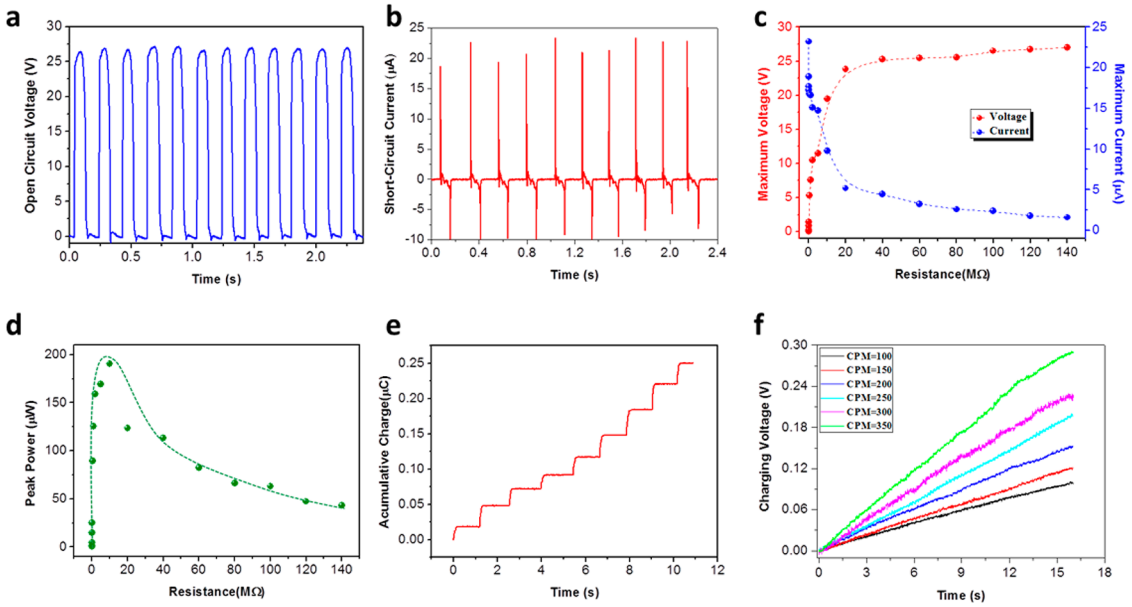

Figure 6. Intelligent keyboard as a self-powered system. (a) Measured open-circuit voltage and (b) short-circuit current of the IKB under the intermittent typing model. (c) Dependence of the voltage and current output on the external load resistance. The points represent the peak values of electrical signals while the lines are the fitted results. (d) Dependence of the peak power output on the external load resistance, indicating maximum power output when R = 9MΩ. (e) Accumulative induced charges generated by the IKB. Each step represents an output current resulting from a keystroke. (f) The IKB can effectively capture the wasted typing energy for charging portable electronics in a wide range of typing speed. A directly proportional relationship was found between the typing speed and the charging rate.

Contact Area Improvement. Aimed at optimizing the output performance when a keystroke is initiated, FEP nanowires arrays were purposely created to enhance the effective contact area between the human finger and FEP surface. In order to give a comprehensive picture of the contact area improvement, first, a SEM characterization of human finger skin shows that the surface has topographical roughness at micro- and even nanoscale, as demonstrated in Supporting Figure S34a. Without FEP nanowires, the contact between the human skin and FEP is possibly confined at certain points due to the surface asperities (Supporting Figure S34b). With an average clustering diameter of 104 ± 21 nm and a length of 0.8 ± 0.2 μm, the FEP nanowires are likely to be readily bent and become adaptive to the morphology of the human finger due to a dimensional matching (Supporting Figure S34c). Such a conformable structural interaction can result in an improvement of the real contact area.

Furthermore, in order to further verify the structural coupling enabled contact area improvement, control experiments were also designed to systematically investigate the influence of FEP nanowires on the electrical output. Likewise, two typing modes, intermittent and continuous typing, were both evaluated. As demonstrated in Supporting Figures S35 and S36, both the open-circuit voltage and short-circuit current were enhanced when typing on the IKB with FEP nanowires surface modification. Factors that may influence the output amplitudes include materials selection, device size, effective contact area, testing condition. While all factors except for the effective contact area can be ruled out. Therefore, enhanced effective contact area resulting from the structural coupling of FEP nanowires and human skin hierarchical roughness is the most likely reason.

In addition, a further step was taken to investigate the relationship between electric output and the applied contacting force. A dual-range force sensor was employed to quantitatively control the applied typing force. As demonstrated in the Figure 7a, for both IKBs, with or without FEP nanowires as surface modification, the current output is clearly increasing with elevated contact forces. However, different increasing trends were found. First, at a fixed applied force, the output of IKB with FEP nanowires is always larger than that of the IKB without FEP nanowires. Second, the output has different force sensitivities. Third, a faster saturation was observed for the IKB without FEP nanowires. These observations are mainly attributed to the increased contact area at larger forces. The surface of human finger skin and FEP are neither absolutely flat nor smooth. At small contacting force, the surface roughness leads to some areas untouched between the FEP and human skin, while a larger pressure could bring the two surfaces a fully intimate contact. The reliance of output on the applied contact force further validates that the enhanced effective contact area is attributed to the structural coupling of FEP nanowires and human skin hierarchical roughness.

Reliability and Reproducibility. The reliability of the IKB is primarily represented by its mechanical durability

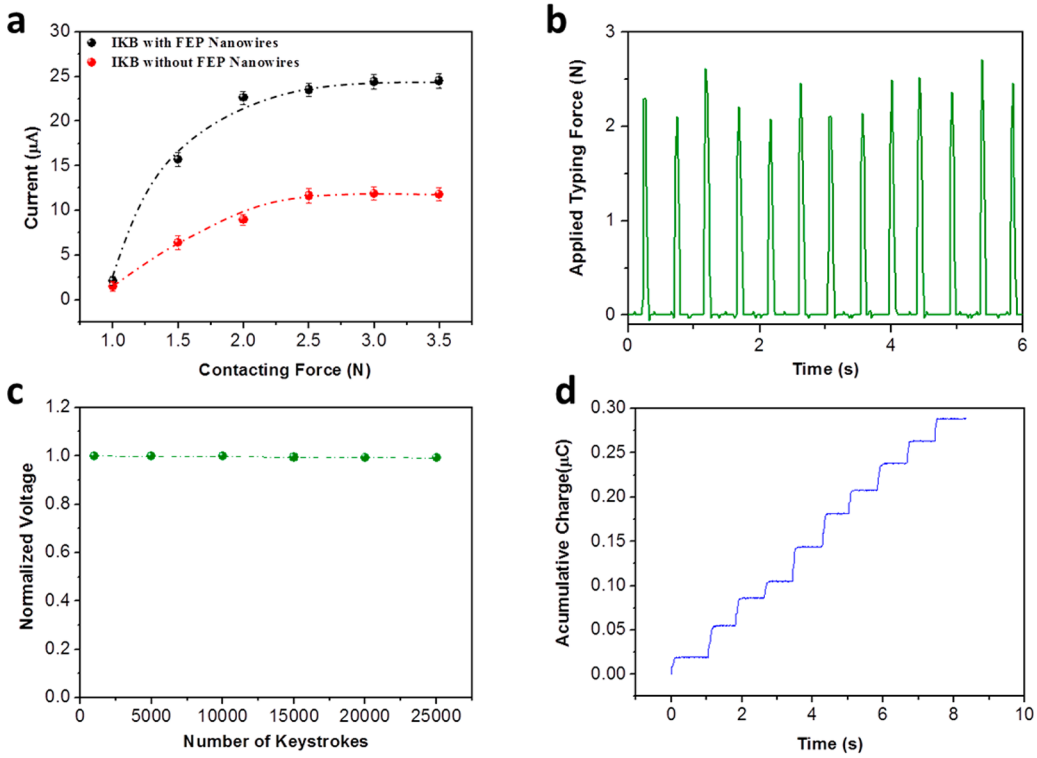

Figure 7. Force dependent output performance of IKB and its reliability test. (a) Investigation of the relationship between electric output and the applied contacting force for IKBs with or without FEP nanowires. (b) The applied typing force to the IKB by an index finger for the mechanical durability test. (c) Mechanical durability test of the IKB. The output voltage only shows a minor fluctuation of less than 0.8% after 25,000 cycles of repetitive keystroke. (d) Accumulative induced charges generated by the intelligent keyboard with wearing a pair of Latex gloves.

and output stability. First, mechanical durability against the applied pressure during the iterative keystrokes has been investigated. The applied typing force by an index finger was fixed at a value of 2.3 ± 0.2 N, as shown in Figure 7b. As demonstrated in Supporting Figure S37, after finger keystrokes for 25,000 cycles, a SEM characterization of the IKB surface shows that the iterative keystrokes do not result in permanent deformation for the vertically standing FEP nanowires. A possible reason is that, for nanowires with proper length of several hundred nanometers, the elastic property ensures retained orientation and morphology of nanowires even after numerous keystrokes.[27] In the meanwhile, as shown in Figure 7c, the output voltage only shows a minor fluctuation of less than 0.8% after 25,000 cycles of repetitive keystrokes. This mechanical robustness along with the output stability is mainly attributed to its robust structure that is consisted of durable thin film materials.

Furthermore, the influence of sweaty hand on the IKB output performance was still investigated. As demonstrated in Supporting Figure S38, after the hands of the typist naturally getting sweaty, there is no observable difference in term of the amplitudes as well as waveshape of both voltage and current signals when he was continuously typing on the intelligent keyboard. Thus, the sweaty hand can barely degrade the output performance of the IKB. In addition, as shown in Supporting Figures S7−S32, all the 104 sets of typing patterns are unique and self-consistent, which further validates the reliability and reproducibility of the IKB.

Additionally, it is worth noting that contact electrification is a universal effect that exists for almost all of the materials, coupling with the surface FEP nanowires enabled superior touching sensitivity, the IKB can effectively respond to either insulating or conductive materials of any kinds, even a glove-wearing intrusion or imposture could be effectively detected. Figure 7d shows the accumulative induced charges generated by the intelligent keyboard with hands wearing a pair of Latex gloves. Each step represents an output current resulting from a keystroke, generating 39 nC of induced charges on average, which is comparable to or even better than the results obtained by directly typing using bare hands.

CONCLUSIONS

Enabled by the contact electrification and electrostatic induction between human fingers and the keys, an innovative intelligent, self-powered keyboard was developed in this work. It can effectively convert the typing motions on the keyboard into local electronic controlling signals, which can be harnessed for either touch-sensing or energy-harvesting purposes. Through integration with a signal-processing circuit, the IKB is

able to trigger a wireless alarm when a keystroke is launched onto the keyboard. This self-securing functionality of the IKB promises greater flexibility for users dealing with intrusions.

A further investigation was conducted to equip the IKB with a customized multi-channel data acquisition system, and the IKB is thus capable of tracing the typing motions and recording the typing contents in real time. Acting as an advanced safeguard against unauthorized access to computer resources, the IKB provides great convenience to security administrators for identifying impostors and intruders.

Furthermore, the IKB is able to identify the personal characters of typing individuals using keystroke dynamics. The triboelectrification induced electric signals by the human typing motions not only relate to the manner and rhythm of the keystroke, but also concern a lot of personalities, such as typing habit, the size of the person's fingers, individual bioelectricity, the applied typing press force, the typing speed, and so on. Consequently, these signals can not only characterize the property of keystroke timing, but also quantitatively record the concrete dynamic changes in the course of typing motions, and thus they provide an unprecedentedly accurate, unique, and permanent typing pattern for further verification and identification purposes. Meanwhile, individual typing patterns are successfully classified and identified using DB4, which justified the effectiveness and practicality of the typing patterns as identifiers. More importantly, a further step was taken to build up a biometric authentication system using the superior typing patterns. A remarkably low Equal Error Rate (EER) value of 1.34% was achieved at the threshold of 0.37. Besides, compared with other biometrics techniques, the triboelectrification enabled behavioral biometric of keystroke dynamics is extremely cost-effective, less intrusive, and user friendly and can be easily implemented as an additional layer of stronger security on current authentication systems without major modification. Thus, the presented IKB in this work is a milestone in keystroke dynamics and a practical step toward highly secured computer systems and networks.

In addition, the IKB is able to convert human typing into electricity. At a moderate typing speed of 350 CPM, the IKB can effectively harness the type motions to generate power and charge a commercial capacitor at a rate of 0.019 V s^{-1}, which provides a feasible means of utilizing the wasted typing energy and has the potential of developing itself into a self-powered working manner. At least, it is capable of extending throughout the runtime of small battery-operated systems, such as remotes, wireless keyboard, and wireless mice. Also, having a surface superhydrophobicity owning to nanostructure modification, the IKB is an effective self-cleaner, which keeps itself free of dirt and grime.

Given its exceptional properties of self-securing, self-powering, and self-cleaning, as well as cost-effectiveness and unique applicability resulting from distinctive mechanism and one-piece non-mechanical-punching structure, the IKB is a practical approach in converting typing motions for either sensing or energy harvesting purposes. Moreover, it is worth noting that, as the most comment input tool today, keyboards widely exist in our daily life, from cash registers to automated banking machines, and from musical instrument to game machines. The justified concepts and demonstrations in this work can be immediately and extensively adopted in a variety of applications, and ultimately improving our way of living.

METHODS

Fabrication of Nanowires Array on FEP Surface. (1) Wash the FEP film ordinally with menthol, isopropyl alcohol, and deionized water, and then dry with compressed nitrogen. (2) Using a DC sputter, coat a 10 nm thick layer of Au onto the FEP film as a nanoscale mask for creating the surface roughness. (3) Put the Au-coated FEP in to ICP chamber, and introduce O_2, Ar, and CF_4 gases into the ICP chamber at flow ratios of 10.0, 15.0, and 30.0 sccm, respectively. (4) Use one power source of 400 W to generate a large density of plasma and another power source of 100 W to accelerate plasma ions toward the FEP surface. (5) ICP reactive ion etching for 60 s.

Fabrication of a KFE. (1) Deposit 100 nm ITO on both sides of a PET substrate of 50 μm thickness using a RF sputter. (2) According to the key distribution of a keyboard, cut the ITO-coated PET substrate into the desired design using a laser cutter, and selectively erase the surface ITO by the laser cutter to form functional electrical pathways. (3) Connect lead wires to the top and bottom ITO electrodes at the end of each pathway. (4) Adhere a FEP thin film (50 μm) on one side of the device as an electrification layer. (5) Use the laser cutter to trim away the redundant part of the FEP layer and make it consistent with the designed PET pattern.

Surface Sliding Angle Measurement. In the tilting base method, sliding angle is the maximum plate tilted angle permitted without increasing the three-phase contact line, when a liquid droplet slides down on an inclined plate. As the surface is inclined, gravity causes the contact angle on the downhill side to increase while the contact angle on the uphill side decreases. Keep increasing the plate titled angle without moving the three-phase contact line to a maximum. This maximum plate tilted angle is the so-called sliding angle. In the experiment, a water droplet with a fixed volume of 10 μL was dispensed onto the IKB surface by a microsyringe, and then the IKB was titled slowly until it reached a critical angle. A surface sliding angle of 7.2° $\pm$ 0.5° was obtained by repeating the measurement ten times.

Customized Multi-Channel Data Acquisition System. The customized multi-channel data acquisition system is mainly consisted of an as-fabricated IKB and a multiplexing analog-to-digital converter. For data acquisition, each key is individually connected *via* a series resistor to a multiplexing analog-to-digital converter, which makes it possible for multi-channel signals to share one A/D converter. The software platform is constructed based on LabView, which is capable of realizing real-time data acquisition control and analysis.

Experimental Setup for Electrical Measurement. (1) Mount the flexible and transparent KFE onto a commercial keyboard. (2) Use a Dual-Range Force Sensor (Vernier Software & Technology, LLC.) to measure the applied typing force by a keystroke to the IKB. (3) Acquire the output voltage signal of the IKB *via* a voltage

preamplifier (Keithley 6514 System Electrometer) and the output current signal of the IKB by a low-noise current preamplifier (Stanford Research SR560).

Conflict of Interest: The authors declare no competing financial interest.

Acknowledgment. Research was supported by U.S. Department of Energy, Office of Basic Energy Sciences (Award DE-FG02-07ER46394), and the "thousands talents" program for pioneer researcher and his innovation team, China, Beijing City Committee of science and technology (Z131100006013004, Z131100006013005). Patents have been filed based on the research results presented in this article. We also thank Simiao Niu for the helpful discussion, Zhaoling Li and Xing Fan for their assistance in collecting the typing patterns, as well as the 104 participants for their contributions of the 104 sets of typing patterns. J.C. expresses his sincere gratitude to the MIT Hayden Library for the quiet and comfortable learning environments.

Supporting Information Available: Figure S1, tilting base method for surface sliding angle measurement; Figure S2, circuit diagram of the complete self-securing system; Figure S3, keys classification in the intelligent keyboard; Figure S4, intelligent keyboard as a self-securing system to trace and record the typing motions; Figure S5, frequency spectra of the typing patterns obtained from the intelligent keyboard; Figure S6, typing patterns after Daubechies Wavelet of order 4 (DB4) transformation; Figures S7−S32, typing patterns and their corresponding D_4 and S_4 components of the 104 participants; Figure S33, accumulative triboelectric charges by the intelligent keyboard under the continuous typing work model; Figure S34, contact area was improvement by FEP nanowires surface modification; Figure S35, electrical output comparison of an IKB in the intermittent tying mode with or without FEP nanowires surface modification; Figure S36, electrical output comparison of an IKB in the continuously typing mode with or without FEP nanowires surface modification; Figure S37, IKB mechanical robustness investigation; Figure S38, influence of sweaty hand on the IKB output performance; Table S1, major components of frequency spectrum of typing patterns; Table S2, triboelectric table; Note S1, analytical derivation of threshold voltage V_{th}; Supporting Movies 1−6 (respectively files si_002−007.avi). This material is available free of charge *via* the Internet at http://pubs.acs.org.

REFERENCES AND NOTES

1. Choo, K.-K. R. The Cyber Threat Landscape: Challenges and Future Research Directions. *Computers & Security* **2011**, *30*, 719–731.
2. Kraemer, S.; Carayon, P.; Clem, J. Human and Organizational Factors in Computer and Information Security: Pathways to Vulnerabilities. *Computers & Security* **2009**, *28*, 509–520.
3. Besnard, D.; Arief, B. Computer Security Impaired by Legitimate Users. *Computers & Security* **2004**, *23*, 253–264.
4. Lowell, J.; Rose-Innes, A. C. Contact Electrification. *Adv. Phys.* **1980**, *29*, 947–1023.
5. Terris, B. D.; Stern, J. E.; Rugar, D.; Mamin, H. J. Contact Electrification Using Force Microscopy. *Phys. Rev. Lett.* **1989**, *63*, 2669–2672.
6. Horn, R. G.; Smith, D. T.; Grabbe, A. Contact Electrification Induced by Monolayer Modification of a Surface and Relation to Acid-Base Interactions. *Nature* **1993**, *366*, 442–443.
7. Horn, R. G.; Smith, D. T. Contact Electrification and Adhesion between Dissimilar Materials. *Science* **1992**, *256*, 362–364.
8. Grzybowski, B. A.; Winkleman, A.; Wiles, J. A.; Brumer, Y.; Whitesides, G. M. Electrostatic Self-Assembly of Macroscopic Crystals Using Contact Electrification. *Nat. Mater.* **2003**, *2*, 241–245.
9. Baytekin, H. T.; Patashinskii, A. I.; Branicki, M.; Baytekin, B.; Grzybowski, B. A. The Mosaic of Surface Charge in Contact Electrification. *Science* **2011**, *333*, 308–312.
10. Liu, C.; Bard, A. J. Electrostatic Electrochemistry at Insulators. *Nat. Mater.* **2008**, *7*, 505–509.
11. Karnan, M.; Akila, M.; Krishnaraj, N. Biometric Personal Authentication Using Keystroke Dynamics: A Review. *Appl. Soft. Comput.* **2011**, *11*, 1565–1572.
12. Gaines, R. S.; Lisowski, W.; Press, S. J.; Shapiro, N. Authentication by Keystroke Timing: Some Preliminary Results, Technical Report R-2526-NSF, RAND Corp., **1980**.
13. Sheng, Y.; Phoha, V. V.; Rovnyak, S. M. A Parallel Decision Tree-Based Method for User Authentication Based on Keystroke Patterns. *IEEE Trans. Syst., Man, Cybern. B, Cybern.* **2005**, *35*, 826–833.
14. Araújo, L. C. F.; Sucupira, L. H. R., Jr.; Lizárraga, M. G.; Ling, L. L.; Yabu-Uti, J. B. T. User Authentication Through Typing Biometrics Features. *IEEE Trans. Sign. Proces.* **2005**, *53*, 851–855.
15. Yu, E.; Cho, S. Keystroke Dynamics Identity Verification-Its Problems and Practical Solutions. *Computers & Security* **2004**, *23*, 428–440.
16. Hwang, S.; Cho, S.; Park, S. Keystroke Dynamics-Based Authentication for Mobile Devices. *Computers & Security* **2009**, *28*, 85–93.
17. Monrose, F.; Rubin, A. D. Keystroke Dynamics as a Biometric for Authentication. *Future Gener. Comp. Syst.* **2000**, *16*, 351–359.
18. Bergadan, F.; Gunetti, D.; Picardi, C. User Authentication through Keystroke Dynamics. *ACM Trans. Inform. Syst. Se.* **2002**, *5*, 367–397.
19. Ahmed, A. A.; Traore, I. Biometric Recognition Based on Free-Text Keystroke Dynamics. *IEEE Trans. Cybern.* **2014**, *44*, 458–472.
20. Chang, T. Y.; Tsai, C. J.; Lin, J. H. A Graphical-Based Password Keystroke Dynamic Authentication System for Touch Screen Handheld Mobile Devices. *J. Syst. Software* **2012**, *85*, 1157–1165.
21. Wacharasindhu, T.; Kwon, J. W. A Micromachined Energy Harvester from a Keyboard Using Combined Electromagnetic and Piezoelectric Conversion. *J. Micromech. Microeng.* **2008**, *18*, 104016.
22. Blossey, R. Self-Cleaning Surfaces-Virtual Realities. *Nat. Mater.* **2003**, *2*, 301–306.
23. Lafuma, A.; Quéré, D. Superhydrophobic States. *Nat. Mater.* **2003**, *2*, 457–460.
24. Tuteja, A.; Choi, W.; Ma, M.; Mabry, J. M.; Mazzella, S. A.; Rutledge, G. C.; Mckinley, G. H.; Cohen, R. E. Designing Superoleophobic Surfaces. *Science* **2007**, *318*, 1618–1622.
25. Fang, H.; Wu, W.; Song, J.; Wang, Z. L. Controlled Growth of Aligned Polymer Nanowires. *J. Phys. Chem. Lett.* **2009**, *113*, 16571–16574.
26. Diaz, A. F.; Felix-Navarro, R. M. A Semi-Quantitative Triboelectric Series for Polymeric Materials: the Influence of Chemical Structure and Properties. *J. Electrostat.* **2004**, *62*, 277–290.
27. Zhu, G.; Pan, C.; Guo, W.; Chen, C.; Zhou, Y.; Yu, R.; Wang, Z. L. Triboelectric-Generator-Driven Pulse Electrodeposition for Micro-patterning. *Nano Lett.* **2012**, *12*, 4960–4965.
28. Meng, B.; Tang, W.; Too, Z.; Zhang, X.; Han, M.; Liu, W.; Zhang, H. A Transparent Single-Friction-Surface Triboelectric Generator and Self-powered Touch Sensor. *Energy Environ. Sci.* **2013**, *6*, 3235–3240.
29. Chen, J.; Zhu, G.; Yang, W.; Jing, Q.; Bai, P.; Yang, Y.; Hou, T.; Wang, Z. L. Harmonic-Resonator-Based Triboelectric Nanogenerator as a Sustainable Power Source and a Self-Powered Active Vibration Sensor. *Adv. Mater.* **2013**, *25*, 6094–6099.
30. Yang, W.; Chen, J.; Zhu, G.; Yang, J.; Bai, P.; Su, Y.; Jing, Q.; Cao, X.; Wang, Z. L. Harvesting Energy from Natural Vibration of Human Walking. *ACS Nano* **2013**, *7*, 11317–11324.
31. Yang, J.; Chen, J.; Liu, Y.; Yang, W.; Su, Y.; Wang, Z. L. Triboelectrification-Based Organic Film Nanogenerator for Acoustic Energy Harvesting and Self-Powered Active Acoustic Sensing. *ACS Nano* **2014**, *8*, 2649–2657.
32. Zhu, G.; Zhou, Y. S.; Bai, P.; Meng, X. S.; Jing, Q.; Chen, J.; Wang, Z. L. A Shape-Adaptive Thin-Film-Based Approach for 50% High-Efficiency Energy Generation Through

Micro-Grating Sliding Electrification. *Adv. Mater.* **2014**, *26*, 3788–3796.
33. Yang, W.; Chen, J.; Jing, Q.; Yang, J.; Wen, X.; Su, Y.; Zhu, G.; Bai, P.; Wang, Z. L. 3D Stack Integrated Triboelectric Nanogenerator for Harvesting Vibration Energy. *Adv. Funct. Mater.* **2014**, *24*, 4090–4096.
34. Yang, J.; Chen, J.; Yang, Y.; Zhang, H.; Yang, W.; Bai, P.; Su, Y.; Wang, Z. L. Broadband Vibrational Energy Harvesting Based on a Triboelectric Nanogenerator. *Adv. Energy Mater.* **2014**, *4*, No. 1301322.
35. Zhu, G.; Bai, P.; Chen, J.; Wang, Z. L. Power-Generating Shoe Insole Based on Triboelectric Nanogenerators for Self-Powered Consumer Electronics. *Nano Energy* **2013**, *2*, 688–692.
36. Zhu, G.; Chen, J.; Zhang, T.; Jing, Q.; Wang, Z. L. Radial-Arrayed Rotary Electrification for High Performance Triboelectric Generator. *Nat. Commun.* **2014**, *5*, No. 3426.
37. Zhou, Y. S.; Liu, Y.; Zhu, G.; Lin, Z.; Pan, C.; Jing, Q.; Wang, Z. L. *In-Situ* Quantitative Study of Nanoscale Triboelectrification and Patterning. *Nano Lett.* **2013**, *13*, 2771–2776.
38. Zhu, G.; Chen, J.; Liu, Y.; Bai, P.; Zhou, Y.; Jing, Q.; Pan, C.; Wang, Z. L. Linear-Grating Triboelectric Generator Based on Sliding Electrification. *Nano Lett.* **2013**, *13*, 2282–2289.
39. Bai, P.; Zhu, G.; Liu, Y.; Chen, J.; Jing, Q.; Yang, W.; Ma, J.; Zhang, G.; Wang, Z. L. Cylindrical Rotating Triboelectric Nanogenerator. *ACS Nano* **2013**, *7*, 6361–6366.
40. Lin, L.; Wang, S.; Niu, S.; Liu, C.; Xie, Y.; Wang, Z. L. Noncontact Free-Rotating Disk Triboelectric Nanogenerator as a Sustainable Energy Harvester and Self-Powered Mechanical Sensor. *ACS Appl. Mater. Interfaces* **2014**, *6*, 3031–3038.
41. Wang, S.; Xie, Y.; Niu, S.; Lin, L.; Wang, Z. L. Freestanding Triboelectric-Layer Based Nanogenerators for Harvesting Energy from a Moving Object or Human Motion in Contact and Non-contact Modes. *Adv. Mater.* **2014**, *26*, 2818–2824.
42. Zhong, J.; Zhong, Q.; Fan, F.; Zhang, Y.; Wang, S.; Hu, B.; Wang, Z. L.; Zhou, J. Finger Typing Driven Triboelectric Nanogenerator and Its Use for Instantaneously Lighting Up LEDs. *Nano Energy* **2013**, *2*, 491–497.
43. Zhong, Q.; Zhong, J.; Hu, B.; Hu, Q.; Zhou, J.; Wang, Z. L. A Paper-Based Nanogenerator as a Power Source and Active Sensor. *Energy Environ. Sci.* **2013**, *6*, 1779–1784.
44. Hu, Q.; Wang, B.; Zhong, Q.; Zhong, J.; Hu, B.; Zhang, X.; Zhou, J. Metal-Free and Non-Fluorine Paper-Based Generator. *Nano Energy* **2014**, 10.1016/j.nanoen.2014.09.036.
45. Niu, S.; Liu, Y.; Wang, S.; Lin, L.; Zhou, Y.; Hu, Y.; Wang, Z. L. Theoretical Investigation and Structural Optimization of Single-Electrode Triboelectric Nanogenerators. *Adv. Funct. Mater.* **2014**, *24*, 3332–3340.
46. Feng, G.; Fan, J. Analysis of Simultaneous Switching Noise Coupling in Multilayer Power/Ground Planes with Segmentation Method and Cavity Model. *IEEE Trans. Electromagn. Compat.* **2010**, *52*, 699–711.
47. Yoo, J.; Yan, L.; El-Damak, D.; Altaf, M. A. B.; Shoeb, A. H.; Chandrakasan, A. P. An 8-Channel Scalable EEG Acquisition SoC with Patient-specific Seizure Classification and Recording Processor. *IEEE J. Solid-State Circuits* **2013**, *48*, 214–228.
48. Ingrid, D. *Ten Lectures on Wavelets*; Society for Industrial and Applied Mathematics: Philadelphia, PA, 1992.
49. Xu, W.; Chang, C.; Hung, Y. S.; Kwan, S. K.; Fung, P. C. W. Order Statistics Correlation Coefficient as a Novel Association Measurement with Applications to Biosignal Analysis. *IEEE Trans. Sign. Process.* **2007**, *55*, 5552–5563.